Cell Research (2011) 21:258-274.

www.nature.com/cr

ORIGINAL ARTICLE

Structural bases of dimerization of yeast telomere protein Cdc13 and its interaction with the catalytic subunit of DNA polymerase α

Jia Sun[1, 2], Yuting Yang[1, 2], Ke Wan[1, 2], Ninghui Mao[3], Tai-Yuan Yu[4], Yi-Chien Lin[4], Diane C DeZwaan[5], Brian C Freeman[5], Jing-Jer Lin[4], Neal F Lue[3], Ming Lei[1, 2]

[1]Howard Hughes Medical Institute; [2]Department of Biological Chemistry, University of Michigan Medical School, 1150 W. Medical Center Drive, Ann Arbor, MI 48109, USA; [3]Department of Microbiology & Immunology, W.R. Hearst Microbiology Research Center, Weill Medical College of Cornell University, 1300 York Avenue, New York, NY 10065, USA; [4]Institute of Biopharmaceutical Sciences, National Yang-Ming University, Shih-Pai 112, Taipei; [5]Department of Cell and Developmental Biology, University of Illinois, 601 South Goodwin Avenue, Urbana, IL 61801, USA

Budding yeast Cdc13-Stn1-Ten1 (CST) complex plays an essential role in telomere protection and maintenance, and has been proposed to be a telomere-specific replication protein A (RPA)-like complex. Previous genetic and structural studies revealed a close resemblance between Stn1-Ten1 and RPA32-RPA14. However, the relationship between Cdc13 and RPA70, the largest subunit of RPA, has remained unclear. Here, we report the crystal structure of the N-terminal OB (oligonucleotide/oligosaccharide binding) fold of Cdc13. Although Cdc13 has an RPA70-like domain organization, the structures of Cdc13 OB folds are significantly different from their counterparts in RPA70, suggesting that they have distinct evolutionary origins. Furthermore, our structural and biochemical analyses revealed unexpected dimerization by the N-terminal OB fold and showed that homodimerization is probably a conserved feature of all Cdc13 proteins. We also uncovered the structural basis of the interaction between the Cdc13 N-terminal OB fold and the catalytic subunit of DNA polymerase α (Pol1), and demonstrated a role for Cdc13 dimerization in Pol1 binding. Analysis of the phenotypes of mutants defective in Cdc13 dimerization and Cdc13-Pol1 interaction revealed multiple mechanisms by which dimerization regulates telomere lengths *in vivo*. Collectively, our findings provide novel insights into the mechanisms and evolution of Cdc13.

***Keywords*:** telomere; polymerase; telomerase

Cell Research (2011) **21**: 258-274. doi:10.1038/cr.2010.138; published online 28 September 2010

Introduction

Telomeres are specialized nucleoprotein structures that maintain the integrity of eukaryotic chromosomal termini by protecting them from fusion and recombination, and promoting their replication [1, 2]. In most organisms, telomeric DNA consists of short repetitive sequences that terminates in 3′ overhangs. Both the double stranded repeats and the 3′ overhangs are bound by a multitude of proteins that are crucial for telomere stability. Moreover, because of incomplete end replication, telomeric DNA has to be periodically replenished following rounds of cell division. This task is primarily performed by a ribonucleoprotein (RNP) known as telomerase, which acts as an unusual reverse transcriptase (RT) [3-5]. Both telomere-binding proteins and telomerase are critical for the maintenance of telomere integrity through multiple cell divisions, which in turn is pivotal in supporting genome stability and promoting cellular life span.

A key element of the telomere nucleoprotein assembly is the protein complex that binds and protects terminal 3′ overhangs (G-tails). One of the best-studied G-tail-binding complex, known as the Cdc13-Stn1-Ten1 (CST) complex, was initially identified and characterized in the budding yeast *S. cerevisiae* [6]. The genes encoding

Correspondence: Ming Lei
E-mail: leim@umich.edu
Received 27 July 2010; revised 13 August 2010; accepted 17 August 2010; published online 28 September 2010

all three components of the complex are essential for cell viability, and hypomorphic alleles of each gene can cause extensive telomere degradation, as well as aberrant telomerase and recombination activities at telomeres. Insights on the mechanisms of this complex have come from analysis of their nucleic acid-binding properties and their interaction partners. Cdc13, the largest subunit, recognizes G-tails with high affinity and sequence specificity through a central OB (oligonucleotide/oligosaccharide binding)-fold domain [7]. This activity is evidently essential for its capping function [8]. Cdc13 also interacts with the telomerase subunit Est1, thereby promoting the recruitment of the entire telomerase RNP to telomere ends [9, 10]. Another binding partner for Cdc13 is Pol1, the catalytic subunit of pol α-primase complex [10, 11]. Loss of Cdc13-Pol1 interaction is correlated with telomere elongation. The DNA-binding activity of Stn1 and Ten1 are less well characterized [12]. Stn1 also interacts with Pol12, another subunit of the pol α-primase complex, which has likewise been implicated in telomere protection and length regulation [13-15].

Although CST was initially believed to be confined to budding yeast, more recent analyses have revealed broad distribution of the Stn1 and Ten1 components across eukaryotic phyla [12, 16-19]. The discovery of these homologs provided added motivations for ascertaining their mechanisms and the extent of their evolutionary conservation. A particularly provocative notion that emerged was the proposal that CST represents a telomere-specific replication protein A (RPA)-like complex [12]. RPA is a nonspecific single-stranded DNA-binding complex that contains three subunits (RPA70, RPA32, and RPA14) and mediates critical and diverse DNA transactions throughout the genome [20, 21]. Structural studies provided compelling support for the resemblance between Stn1 and RPA32, and that between Ten1 and RPA14 [22, 23]. The two protein pairs share many structural features and utilize similar motifs for mutual interactions. Stn1 and RPA32, each consists of an N-terminal OB fold and one or two C-terminal WH motifs, whereas Ten1 and RPA14 each consists of a single OB fold. Complex formation in each case is mediated predominantly through α-helices located at the C-termini of OB folds. Thus, the Stn1-Ten1 subcomplex can plausibly be viewed as a telomere-specific paralog of the RPA32-RPA14 complex. That Stn1 and Ten1 together act as a close-knit unit is further underscored by their ability to function in the absence of Cdc13. Overexpression of Stn1N (the N-terminal OB fold of Stn1) and Ten1 allows the cells to bypass the essential function of Cdc13 and remain viable [14]. By contrast, even though Cdc13 and RPA70 are both large proteins that have either been shown or proposed to contain multiple OB folds, their evolutionary kinship is less clear [21, 24]. Sequence comparison failed to disclose any convincing similarity between the two families, and the DNA-binding OB fold of Cdc13 does not appear to be closely related to the equivalent OB folds in RPA70 [25, 26].

In this report, we provide structural and biochemical analyses of the N-terminal domain of Cdc13. The atomic resolution structure confirmed the existence of an OB fold at the N-terminal end of Cdc13. Both structural and biochemical analyses revealed unexpected dimerization by the N-terminal OB fold. We also uncovered the structural basis of interaction between the N-terminal OB fold and Pol1, and demonstrated a role for N-terminal dimerization in Pol1 binding. Analysis of the phenotypes of mutants defective in Cdc13 dimerization and Cdc13-Pol1 interaction revealed multiple mechanisms by which dimerization regulates telomere lengths *in vivo*. Our findings thus offer novel insights into Cdc13 mechanisms and evolution.

Results

Prediction of four tandem OB-fold domains in Cdc13

To initiate a comparative analysis of Cdc13 and to uncover possible structural domains in this protein, we systemically searched the NCBI and Broad Institute databases for homologs of Cdc13 using available sequences as queries. This resulted in the identification of many Cdc13 homologs in the *Saccharomyces* and *Kluyveromyces* branches of budding yeast (which also include *Candida glabrata*, but not other *Candida* spp.; Supplementary information, Figure S1). Multiple sequence alignment of these Cdc13 proteins clearly revealed a pattern of four conserved regions, each of which spans about 150-200 residues (Supplementary information, Figure S1). These regions in *Saccharomyces cerevisiae* Cdc13 (*Sc*Cdc13) consist of residues 1-231, 323-485, 490-701, and 712-924, respectively (Supplementary information, Figure S1). Notably, the third conserved region coincides with the DNA-binding domain of *Sc*Cdc13 (*Sc*Cdc13$_{DBD}$) [26]. For simplicity, hereafter, *Sc*Cdc13 is referred to as Cdc13.

We next performed a secondary structural analysis on the four conserved regions of Cdc13 using the program PredictProtein [27]. Supporting the validity of this approach, the program accurately predicted the positions of most of the α-helices and β-strands in Cdc13$_{DBD}$ (Supplementary information, Figure S1). This analysis also predicted that each of the three remaining regions contains a β-strand-rich core that exhibits a secondary structure pattern of β−β−β−α−β−β (Supplementary information,

Figure S1), which is characteristic of OB folds found in many telomere proteins including Stn1 and Ten1 [23]. Sequence analyses of several Cdc13 proteins from other yeast species also predicted the existence of four β-strand-rich OB-fold-like domains (data not shown). The less-conserved fragment between the first and the second putative OB folds (~90 resides) exhibited few detectable features of secondary structure (Supplementary information, Figure S1). Notably, this region, called the recruitment domain (RD), has been reported to play an important role in telomerase recruitment through a direct interaction with Est1 (Figure 1) [9, 10].

The largest subunit of the RPA complex, RPA70, also contains four tandem OB-fold domains (Figure 1) [25, 28-30]. Furthermore, there is also an ~60-residue unstructured region between the first and second OB folds in RPA70 (Figure 1). Both features match well with our bioinformatic analysis of Cdc13 (Figure 1 and Supplementary information, Figure S1). Thus, although there is no primary sequence similarity between Cdc13 and RPA70, the similar domain organization of the two proteins supports the view that Cdc13 is a telomere-specific

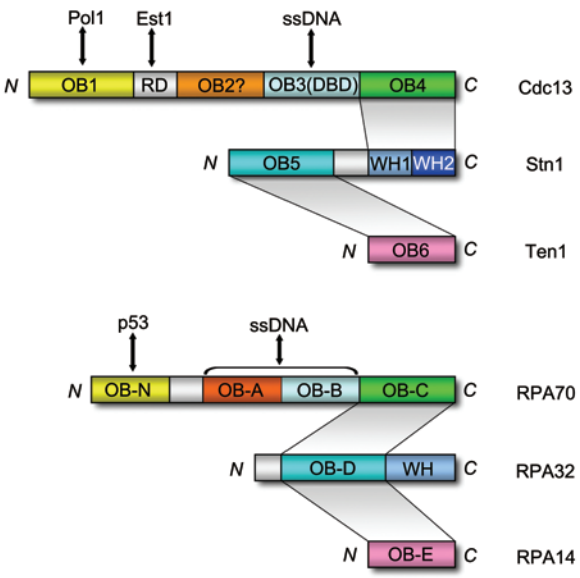

Figure 1 Domain organization of the CST and the RPA complexes. Upper panel: the CST complex; lower panel: the RPA complex. In both Cdc13 and RPA70, the four OB folds from the N- to C-terminus, are colored in yellow, orange, light blue, and green, respectively. The RD domain between the first and second OB folds in Cdc13 is colored in gray. In both Stn1 and RPA32, the OB folds are colored in cyan, the WH1 motif of Stn1 and WH motif of RAP32 in marine, and the WH2 motif of Stn1 in blue. Ten1 and RPA14 are colored in pink. The shaded areas are used to indicate the interdomain interactions among the components within each complex.

RPA70-like protein. However, because OB folds are well known for the absence of reliable primary sequence features that can be used for accurate prediction [31-33], decisive confirmation of the existence of four tandem OB folds in Cdc13 and the similarity between Cdc13 and RP70 requires structural characterization of Cdc13.

Structure of a Cdc13$_{OB1}$ monomer

To address whether Cdc13 contains an OB fold at the N-terminus, recombinant Cdc13$_{OB1}$ (residues 13-243) expressed from *Escherichia coli* was crystallized, and the structure was determined by single anomalous dispersion (SAD) using a mercury compound (MeHgAc) at a resolution of 2.5 Å (Supplementary information, Table S1). The final atomic model, refined to an *R*-value of 21.1% (R_{free} = 26.7%), contains residues 14-225. No electron density is observed corresponding to three loop regions (residues 59-67, 105-111, and 161-170), as well as the C-terminal 18 residues, which we presume to be disordered in solution.

The crystal structure demonstrates that the core of Cdc13$_{OB1}$ is indeed made up of an OB fold, consisting of a highly curved five-stranded antiparallel β-barrel with three peripheral α-helices, as expected from our sequence analysis (Figure 2A). Cdc13$_{OB1}$ contains a large insertion between helix αB and strand β4 (residues 97-124), part of which forms a short β-strand (β3′) that runs antiparallel to β1 before rejoining to β4. In addition, there is a three-helix bundle at the C-terminus, which packs against the convex side of the β-barrel.

Compared with Cdc13$_{OB1}$, the N-terminal OB fold of RPA70 (RPA70N) only contains a β-barrel core and lacks the C-terminal helix bundle (Figure 2B); the size of RPA70N (120 residues) is only about half of that of Cdc13$_{OB1}$ (225 residues). Although the sequences of Cdc13$_{OB1}$ and RPA70N are markedly divergent and share only 8% identity, the β-barrel core of the Cdc13$_{OB1}$ closely resembles that of RPA70N (Figure 2B); the two domains can be superimposed with a root-mean-square deviation (r.m.s.d.) of 3.7 Å for 84 equivalent Cα pairs (Figure 2B) [28, 34]. Not withstanding this similarity, there are substantial structural differences evident in the loop and helix regions. Most notably, the αB helix between strands β3 and β4 of Cdc13$_{OB1}$ is much longer and rotates about 45° away from strand β5 relative to the position of αB in RPA70N, resulting in a large hydrophobic groove between αB and β5 (Figure 2B). This displacement of helix αB is essential for the dimeric conformation of Cdc13$_{OB1}$, as described below (Figure 2C).

Unexpectedly, the structure of Cdc13$_{OB1}$ closely resembles that of Cdc13$_{OB3(DBD)}$ (Supplementary information, Figure S2A). Indeed, an unbiased search for struc-

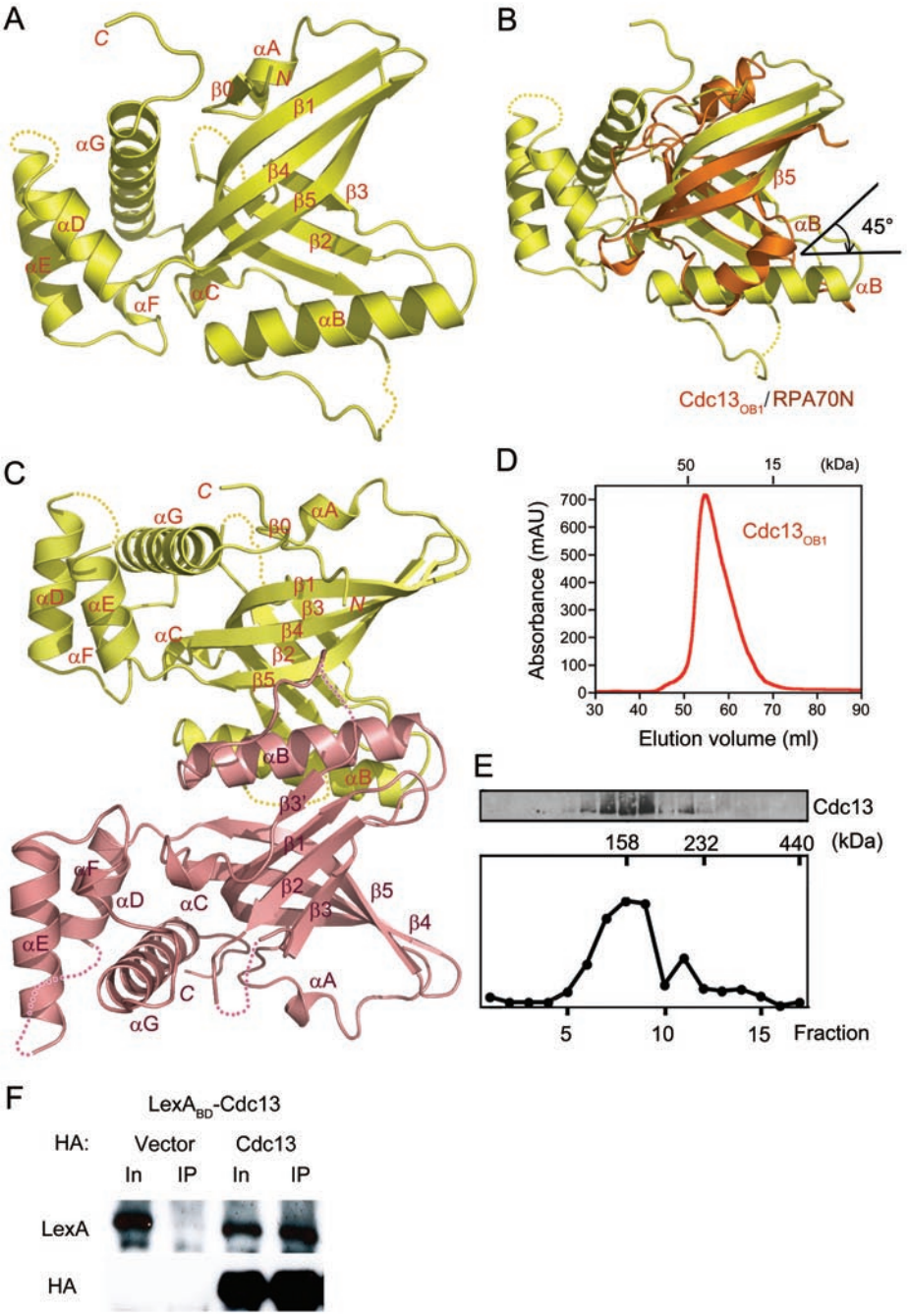

Figure 2 $Cdc13_{OB1}$ forms a dimer, both in crystals and in solution. **(A)** Ribbon diagram of the monomeric structure of $Cdc13_{OB1}$. The secondary structure elements are labeled. In addition to the central β-barrel, there is a helical bundle at the C-terminus packing on one side of the OB fold. **(B)** Superposition of $Cdc13_{OB1}$ (yellow) on the crystal structure of RPA70N (orange) [28]. The αB helix in $Cdc13_{OB1}$ is long and rotates ~45° relative to the orientation of αB in RAP70N. **(C)** Ribbon diagram of the $Cdc13_{OB1}$ dimer. The two subunits are colored in yellow and salmon, respectively. **(D)** Gel-filtration profile revealed that $Cdc13_{OB1}$ behaves as an assembly with an apparent molecular weight of ~45 kDa. **(E)** Full-length Cdc13 was subjected to a sucrose gradient analysis. The distribution of Cdc13 in the gradient was analyzed by western blot using polyclonal antibodies raised against Cdc13 (upper panel). The band intensities were quantified and plotted (lower panel). Sedimentation positions of three standard proteins are also indicated. **(F)** Co-IP of Cdc13 fused to different tags in whole cell lysate. Yeast cells transformed with plasmids expressing $LexA_{BD}$-Cdc13 and HA-Cdc13 were lysed, and IPs were performed using the anti-HA antibody. The levels of each protein in the input and IP samples were analyzed by immunoblotting with the indicated antibodies. Lanes marked ''In'' contain 5% of the input lysate used for the IPs.

turally homologous proteins using the Dali server [35] revealed that the structure of $Cdc13_{OB1}$ is most similar to that of $Cdc13_{OB3}$, with a *Z*-score of 10.3; the two domains can be superimposed with an r.m.s.d. of 3.0 Å for 144 equivalent Cα pairs (Supplementary information, Figure S2A) [26]. However, $Cdc13_{OB3}$ has a very long loop (28 residues), L_{23}, between strands β2 and β3, which packs on one side of the β-barrel and constitutes almost half of the DNA-binding surface (Supplementary information, Figure S2A) [26, 36]. In contrast, strands β2 and β3 of $Cdc13_{OB1}$ are connected by a much shorter loop (12 residues) that is partially disordered in the current structure (Figure 2A).

Cdc13 is a dimer

In the $Cdc13_{OB1}$ crystals, only one $Cdc13_{OB1}$ molecule is present in each asymmetric unit. However, careful examination of the crystal packing of one protomer against its neighbors revealed that $Cdc13_{OB1}$ makes extensive interactions with one of the crystallographic symmetry-related molecule. The two αB helices from both molecules form a tightly packed parallel coiled-coil, whose axis coincides with a crystallographic symmetry dyad (Figure 2C). The $Cdc13_{OB1}$ dimer interface buries a total of ~2 560 $Å^2$ solvent-accessible surface area, which is substantially larger than other crystal-packing contacts. This strongly implies that the dimeric conformation observed in the crystals is unlikely to be the result of lattice packing.

We next asked whether Cdc13 forms a homodimer in solution. Experiments using calibrated gel-filtration chromatography showed that the elution peak of $Cdc13_{OB1}$ corresponded to a molecular weight of about 45 kDa (Figure 2D), as expected if the crystallographic dimer interaction is present in solution. In addition, chemical cross-linking assays with both the OB1 domain and full-length Cdc13 demonstrated that, in both cases, only one higher-molecular-weight band appeared in the presence of cross-linking reagent and the size of this band matched well with a dimer of $Cdc13_{OB1}$ or full-length Cdc13, respectively (Supplementary information, Figure S2B, S2C and S2D). These results corroborated our crystallographic finding, showing that Cdc13 indeed exists as a dimer in solution. The molecular weight of purified full-length Cdc13 was also estimated by sucrose gradients. Cdc13 expressed and purified from insect cells behaves as an assembly with an apparent molecular weight of ~160-170 kDa (Figure 2E). Even though this is less than the expected value of a Cdc13 dimer (210 kDa), it is consistent with our prediction that Cdc13 has a multidomain elongated architecture, which should result in a smaller sedimentation coefficient and thus a reduced apparent molecular mass. To further study the *in vivo* oligomeric state of Cdc13, we tested the dimeric interaction of Cdc13 in yeast cells. Co-immunoprecipitation (Co-IP) experiments with two differently tagged full-length Cdc13 proteins demonstrated that Cdc13 indeed forms a complex with itself in cells (Figure 2F). Finally, we examined the potential role of other Cdc13 domains in dimerization by yeast two-hybrid assays (Supplementary information, Figure S2E). Self-association was not observed for any other domains, indicating that Cdc13 probably forms a homodimer solely through its N-terminal OB fold.

The dimer interface of $Cdc13_{OB1}$

The core of the symmetric dimer interface is mediated primarily by helix αB and strand β5 from both $Cdc13_{OB1}$ subunits (Figure 2C). Together, αB and β5 from one subunit form a hydrophobic groove that accommodates the αB helix from the other (Figure 3A). At one side of the groove, the coiled-coil hydrophobic packing contact between the two αB helices is extensive, consisting of four layers of two-fold symmetry-related interdigitating residues at positions *a* and *d* of the heptad repeats from both helices (Ser81, Leu84, Leu91, and Tyr95) (Figure 3B). These residues stack closely against each other both within and between adjacent layers. In addition, several hydrophobic residues (Phe142, Leu143, Ile146, and Pro148) of β5 from one monomer make close contacts with helix αB from the opposing monomer so that, except for the two termini, helix αB is almost completely buried into the central core of the dimer (Figure 3B and Supplementary information, Figure S3).

Although the dimeric interface is predominantly hydrophobic, intermolecular electrostatic interactions provide additional specificity and stability to the dimer. In the loop regions before the αB helices in both monomers, two symmetry-related Lys77-Asp78 pairs contribute four salt bridges, sealing one end of the interface (Figure 3B). In the center of the coiled-coil, two Thr88 residues form an intermolecular hydrogen bond instead of hydrophobic contacts at position *a* of the heptad (Figure 3B). At the side of helix αB, away from the coiled-coil interface, the hydroxyl group of Ser90 mediates an electrostatic interaction with Asp145 from strand β5 of the opposing $Cdc13_{OB1}$ monomer, helping anchor the αB helix into the hydrophobic groove (Figure 3B). Besides the helix αB-binding groove, we also observed a second smaller interface between the two monomers (Figure 3C). Two acidic residues Asp102 and Asp104 in the loop region between αB and β3′ from one monomer form an extensive electrostatic network containing a total of six salt bridges with the side chains of Arg15 and Lys129 from the other

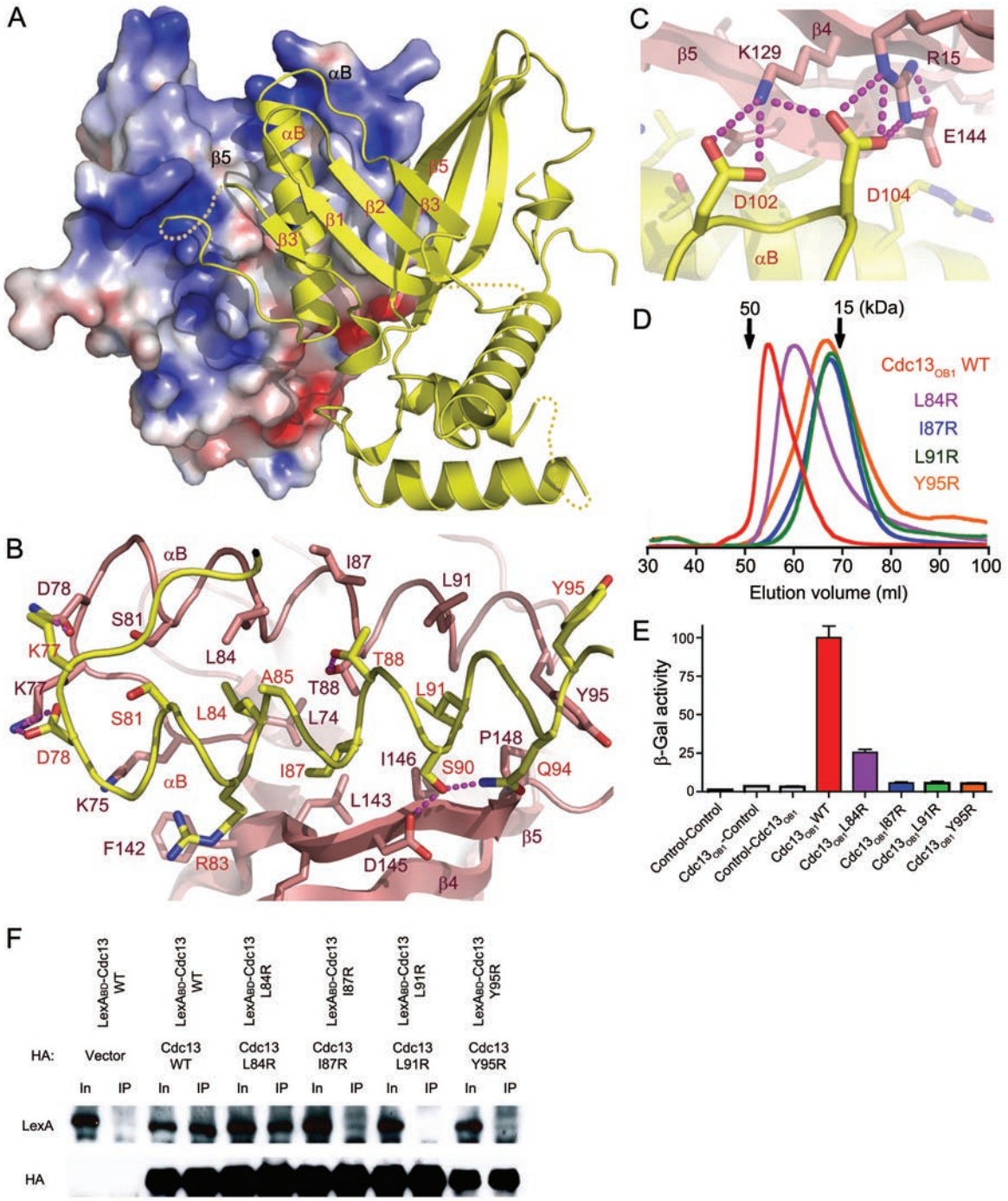

Figure 3 The $Cdc13_{OB1}$ dimer interface. **(A)** The hydrophobic dimer interface. One $Cdc13_{OB1}$ molecule is in surface representation and colored according to its electrostatic potential (positive potential, blue; negative potential, red). The other molecule is in ribbon representation and colored in yellow. **(B)** Helix αB of one $Cdc13_{OB1}$ molecule (in yellow) binds into a hydrophobic groove formed by helix αB and strand β5 of the other (in salmon) in the dimer. Residues important for dimerization are shown as stick models. **(C)** The second interface between the two subunits involves two acidic residues (Asp102 and Asp104) from one $Cdc13_{OB1}$, and two basic residues (Arg15 and Lys129) from the other. **(D)** Superposed chromatographs of wild-type $Cdc13_{OB1}$ and four mutants from gel-filtration columns. **(E)** Effects of four mutations on dimer formation of $Cdc13_{OB1}$ in yeast two-hybrid assays. The color scheme is the same as in **D**. Dimeric interaction between LexA-$Cdc13_{OB1}$ and GAD-$Cdc13_{OB1}$ was determined by measuring the β-galactosidase activity produced by the reporter gene. Data are averages of three independent β-galactosidase measurements normalized to the wild-type dimeric interaction, arbitrarily set to 100. **(F)** Co-IP of the same sets of Cdc13 mutants as in panels **D** and **E** in whole cell lysate. Conditions are the same as in Figure 2F.

monomer (Figure 3C).

To confirm the significance of the dimeric contacts observed in the crystal structure, we generated four missense mutations in $Cdc13_{OB1}$. All mutant proteins were purified to homogeneity, and the oligomeric states of these proteins were individually analyzed by gel-filtration chromatography (Figure 3D). Consistent with the structure, substitution of Ile87, Leu91, or Tyr95 of $Cdc13_{OB1}$ at the hydrophobic interface with a positively charged and bulky arginine residue completely disrupted the dimeric state of the wild-type protein; the elution profiles of these three mutants shifted toward the monomer species on gel filtration (Figure 3D). Notably, the L84R mutant had an elution peak between those of the wild-type $Cdc13_{OB1}$ and the monomer mutants, suggesting that this mutant only weakened but did not disrupt the dimeric interface (Figure 3D). The effects of these mutants were also confirmed by yeast two-hybrid and Co-IP analyses in yeast cells (Figure 3E and 3F). Taken together, we therefore conclude that hydrophobic contact is the major driving force for dimer formation of Cdc13, both *in vitro* and *in vivo*.

Cdc13 dimerization affects cell growth and telomere length regulation

To determine if dimerization affects the function of Cdc13 *in vivo*, we used a plasmid shuffling system developed previously to study the *in vivo* consequences of Cdc13 mutations [10, 11]. We generated yeast strains that carried nondimeric alleles of *CDC13*. These alleles contained either a single (L91R) or quadruple (4R: L84R/I87R/L91R/Y95R) mutations shown earlier to disrupt the OB1 dimer interface. Gel-filtration profile showed that the quadruple mutant protein was well folded and adopted a monomeric conformation in solution (Supplementary information, Figure S4A). Both proteins were expressed at near wild-type levels in yeast cells (Supplementary information, Figure S4B), suggesting that residues at the Cdc13 dimeric interface are not required for protein stability. Interestingly, these strains exhibited no apparent growth defects in comparison to the wild-type control at 30 °C, but manifested a moderate reduction in growth at 37 °C (Figure 4A). Cdc13 dimerization is thus not essential for cell viability, but appears to promote its function at higher temperatures. Analysis of telomere lengths in both mutant clones revealed a consistent and moderate reduction in average telomere lengths (by ~150 bp) (Figure 4B). This reduction was observed about 40 generations following the eviction of plasmids carrying wild-type *CDC13*, and was stable thereafter (data not shown). We also analyzed the level of G-tails in the Cdc13 mutants and observed no detectable increase over that of the wild-type control (Supplementary information, Figure S4C). Collectively, we conclude that Cdc13 dimerization is not essential for cell viability, but is critical for telomere length regulation.

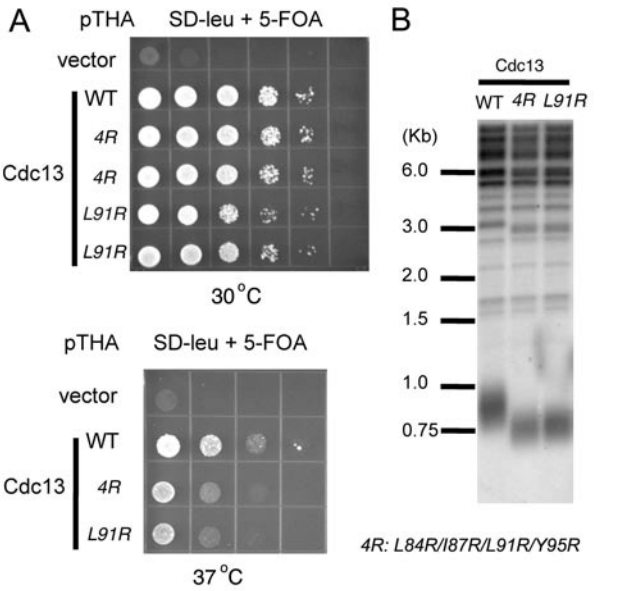

Figure 4 Analysis of Cdc13 dimerization mutants *in vivo*. **(A)** Serial dilutions (10-fold) of strains bearing empty vector or wild-type or mutant CDC13 were spotted on the SD-leu+5-fluoroorotic acid (5-FOA) plates, grown at 30 °C or 37 °C for 2 days, and then photographed. **(B)** Chromosomal DNAs were prepared from strains bearing wild-type or the Cdc13 mutants that are deficient in homodimerization, digested with *Pst*I, and subjected to Southern blot analysis using labeled poly(dG-dT) • poly(dC-dA) as the probe.

Characterization of the Cdc13-Pol1 interaction

Although $Cdc13_{OB1}$ is structurally most similar to $Cdc13_{OB3}$ and also contains a basic cleft that corresponds to the canonical nucleic acid-binding pocket of OB folds, $Cdc13_{OB1}$ does not possess DNA-binding activity (data not shown). Instead, it has been reported to mediate protein-protein interactions at telomeres [10, 11]. One of the $Cdc13_{OB1}$-binding protein is Pol1, the catalytic subunit of DNA polymerase α-primase complex. Disruption of the Cdc13-Pol1 interaction causes cell growth defect and telomere lengthening [10, 11]. An N-terminal region of Pol1 (residues 13-392 reported in one study and residues 47-560 in another) interacts with $Cdc13_{OB1}$ [10, 11]. To determine the mechanism of Pol1 recognition by Cdc13, we characterized the Cdc13-Pol1 interaction by isothermal titration calorimetry (ITC) (Figure 5A). Our data revealed that a short fragment of Pol1 consisting only of residues 215-250 was necessary and sufficient

for binding with $Cdc13_{OB1}$ (Figure 5A). $Cdc13_{OB1}$ binds to $Pol1_{215-250}$ with an equilibrium dissociation constant (K_d) of 3.8 μM (Figure 5B). Hereafter, we will refer to $Pol1_{215-250}$ as $Pol1_{CBM}$ (*C*dc13-*b*inding *m*otif).

Structural basis for the $Cdc13_{OB1}$-$Pol1_{CBM}$ interaction

To characterize the structural basis of Pol1 recognition by Cdc13, we crystallized the $Cdc13_{OB1}$-$Pol1_{CBM}$ complex and solved its structure by molecular replacement at a resolution of 2.4 Å (Supplementary information, Table S1). Except for one residue at the N-terminus and five residues at the C-terminus, $Pol1_{CBM}$ is well ordered, as evidenced by good electron density in the crystals and low temperature factors in the final atomic model. The complex structure has been refined to an *R*-value of 22.4% (R_{free} = 26.4%) with good geometry. The $Cdc13_{OB1}$-$Pol1_{CBM}$ complex structure exhibits a 2:2 stoichiometry between $Cdc13_{OB1}$ and $Pol1_{CBM}$ (Figure 5C). Each $Pol1_{CBM}$ peptide is folded into a single amphipathic α-helix that binds into the deep basic groove mostly formed by one $Cdc13_{OB1}$ monomer (Figure 5C). The $Cdc13_{OB1}$-$Pol1_{CBM}$ interaction does not interfere with the dimeric interface of $Cdc13_{OB1}$ (Figure 5C). The formation of the binary complex causes the burial of ~1 997 Å^2 of surface area at the interface.

Strikingly, the binding mode of $Pol1_{CBM}$ to $Cdc13_{OB1}$ resembles the interaction between RPA70N and p53 (Figure 5D) [28]. In both complexes, a short fragment of one protein ($Pol1_{CBM}$ and $p53_{38-57}$) adopts a helical conformation and binds into the basic groove of the OB fold of the other component in the complex ($Cdc13_{OB1}$ or RPA70N). Notably, canonical ssDNA-binding OB folds employ exactly the same basic groove for DNA association, as illustrated by the structure of the $Cdc13_{OB3}$-ssDNA complex (Figure 5E) [36]. In these structures, both basic and aromatic residues on the ssDNA-binding grooves are required for the interaction; basic residues stabilize the negative phosphate groups of the DNA backbone, whereas aromatic residues are involved in stacking with the bases of the DNA [25, 36-39]. In comparison, although the $Pol1_{CBM}$-binding surface of $Cdc13_{OB1}$ contains many basic residues, there are very few aromatic residues at the expected positions for optimal ssDNA interaction. This is consistent with our data that even at a high protein concentration (~0.5 mM), no $Cdc13_{OB1}$-ssDNA complex was observed in an Electrophoretic Mobility Shift Assay (data not shown). Thus, we conclude that the N-terminal OB fold of Cdc13 is a protein-protein interaction module.

The $Cdc13_{OB1}$-$Pol1_{CBM}$ interface

In the $Cdc13_{OB1}$-$Pol1_{CBM}$ complex structure, the two $Pol1_{CBM}$ peptides adopt symmetric conformations and each $Pol1_{CBM}$ interacts with both $Cdc13_{OB1}$ molecules in the dimer (Figure 5C). The C-terminal half of $Pol1_{CBM}$ contacts with one $Cdc13_{OB1}$ monomer and this interaction is primarily mediated by a highly positively charged cleft of $Cdc13_{OB1}$ dimer and a negatively charged convex surface of the $Pol1_{CBM}$ helix (Figure 6A). The acidic surface of $Pol1_{CBM}$ at the interface contains five negatively charged residues, Asp229, Asp232, Asp236, and Glu238 (Figure 6A). The more extensive basic groove of $Cdc13_{OB1}$ consists of six lysine residues at positions 30, 50, 73, 75, 77, and 135 (Figure 6A). These two surfaces are not only opposite in charge distribution but also complementary in shape. While electrostatic interactions should favor the initial apposition of the two proteins, the interaction specificity between $Cdc13_{OB1}$ and $Pol1_{CBM}$ is mainly provided by van der Waals contacts (Figure 6B). The hydrophobic portion of the amphipathic helix of $Pol1_{CBM}$ packs against the hydrophobic floor of the groove formed by strands β1, β4, and β5 of $Cdc13_{OB1}$, accounting for about half of the total buried surface area (Figure 6B). The core of this hydrophobic interface consists of the side chains of eight residues, Val230, Leu233, Leu234, and Val237 in $Pol1_{CBM}$, and Ile32, Tyr133, Thr140, and Phe143 in $Cdc13_{OB1}$ (Figure 6B). In addition to the helix, the C-terminal tail of $Pol1_{CBM}$ also contributes to the binding to $Cdc13_{OB1}$; it makes a turn at Pro241 and lines the rest of $Pol1_{CBM}$ in an antiparallel direction to strand β5 of $Cdc13_{OB1}$ (Figure 6B). The side chains of Val242 and Val243 pack against a hydrophobic patch of $Cdc13_{OB1}$ formed by residues from strands β3 and β5 (Figure 6B). This conformation is further stabilized by four hydrogen-bonding interactions between $Pol1_{CBM}$ and $Cdc13_{OB1}$ (Figure 6B).

The N-terminal half of the $Pol1_{CBM}$ helix (Pro216-Asp229) protrudes outside the major $Cdc13_{OB1}$-$Pol1_{CBM}$ interface to make direct contacts with the other $Cdc13_{OB1}$ molecule in the dimer (Figure 6B and 6C). In this region of the complex, the $Cdc13_{OB1}$-$Pol1_{CBM}$ interface is also dominated by electrostatic interactions; there are a total of seven salt-bridge and hydrogen-bonding interactions between $Pol1_{CBM}$ and $Cdc13_{OB1}$ (Figure 6B and 6C). Based on the structure, disruption of the dimeric state of $Cdc13_{OB1}$ would result in a loss of ~596 Å^2 of the buried interface area between $Cdc13_{OB1}$ and $Pol1_{CBM}$, suggesting that dimerization of $Cdc13_{OB1}$ might be important for $Pol1_{CBM}$ interaction.

Both the Cdc13-Pol1 interface and Cdc13 dimerization are required for the Cdc13-Pol1 interaction

Our structural analysis provides plausible explanations for previous mutagenesis data of the Cdc13-Pol1 interaction. Two point mutations of Pol1, D236N and P241T,

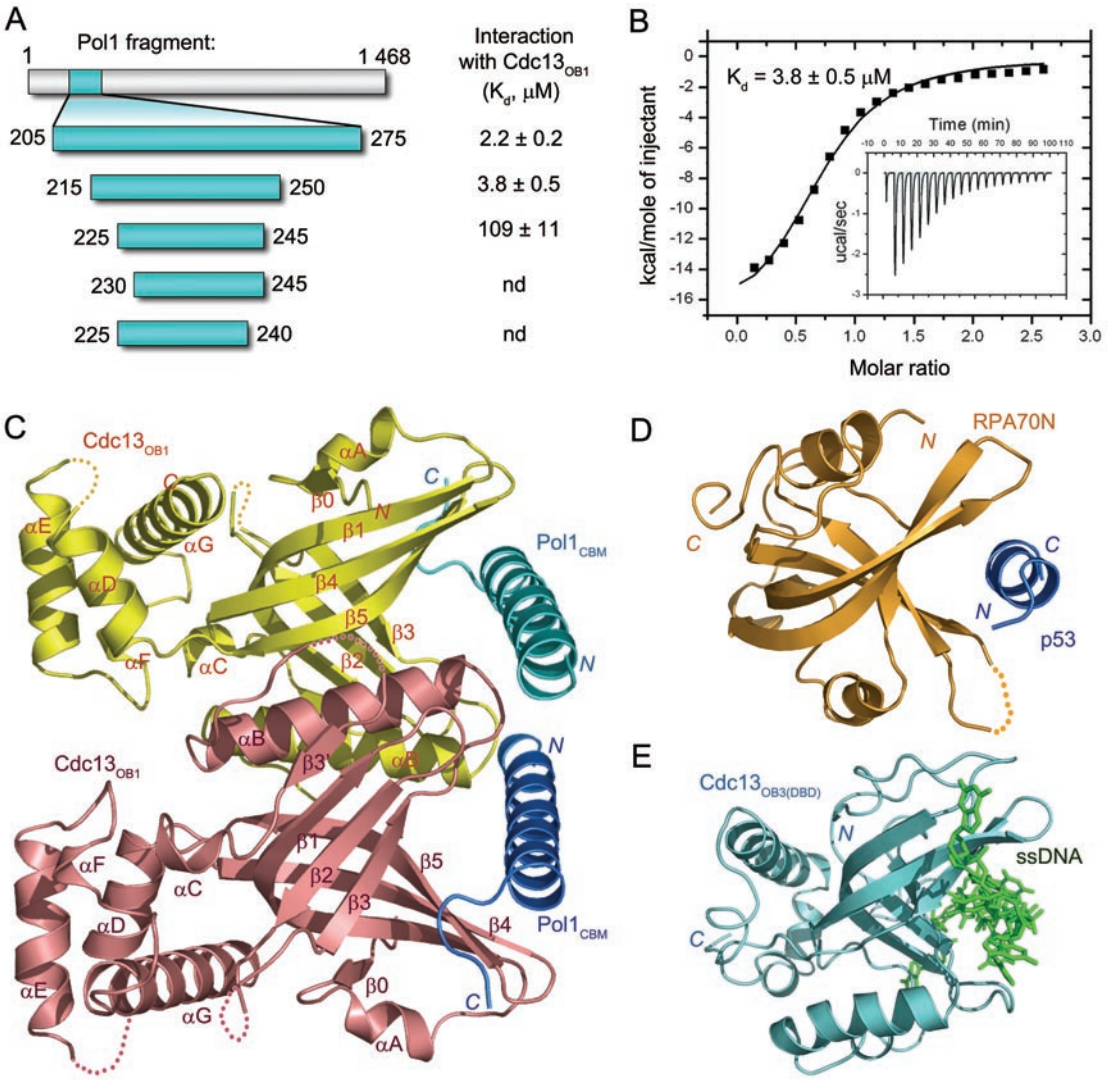

Figure 5 The $Cdc13_{OB1}$-$Pol1_{CBM}$ complex structure. **(A)** Summary of ITC analysis of the interaction between $Cdc13_{OB1}$ and various Pol1 fragments (nd: not detectable by ITC). A short peptide of Pol1 (residues 215-250) was found to be necessary and sufficient for binding to $Cdc13_{OB1}$. **(B)** ITC measurement of the interaction of $Cdc13_{OB1}$ with the $Pol1_{CBM}$ peptide. Insert represents the ITC titration data. The binding curve was fit to a one binding site per $Cdc13_{OB1}$ monomer model. **(C)** Overall structure of the dimeric $Cdc13_{OB1}$-$Pol1_{CBM}$ complex. The two $Cdc13_{OB1}$ molecules are colored as in Figure 2C. The two $Pol1_{CBM}$ peptides are colored in cyan and blue, respectively. 30 amino acids of the $Pol1_{CBM}$ peptide (residues 216-245) are visible in the electron density map. **(D)** The crystal structure of the RPA70N-p53 complex (PDB ID: 2B3G) [28]. **(E)** The NMR structure of the $Cdc13_{OB3}$-ssDNA complex (PDB ID: 1S40) [36]. In **C**, **D**, and **E**, the OB fold of $Cdc13_{OB1}$, RPA70N, and $Cdc13_{OB3}$ are shown in the same orientation. The interacting partners ($Pol1_{CBM}$, p53, and ssDNA) bind to the same basic grooves of the OB folds.

were reported to abolish the interaction [10]. In the crystal structure, the side chain of Pol1 Asp236 points toward the interface and makes two salt bridges with the amino group of Cdc13 Lys73, whereas the unusual backbone dihedral angles of Pol1 Pro241 allows the C-terminus of $Pol1_{CBM}$ to align with Cdc13 strand β5 for optimal interaction (Figure 6B). A third mutation of Pol1, E238K, weakened but did not abolish the interaction [10]. This is also consistent with the structure: the side chain of Glu238, exposed to the solvent, contributes only one hydrogen-bonding interaction (Figure 6B).

To further examine the significance of the $Cdc13_{OB1}$-$Pol1_{CBM}$ interface, we assessed the effects of an additional panel of mutations in either $Cdc13_{OB1}$ or $Pol1_{CBM}$

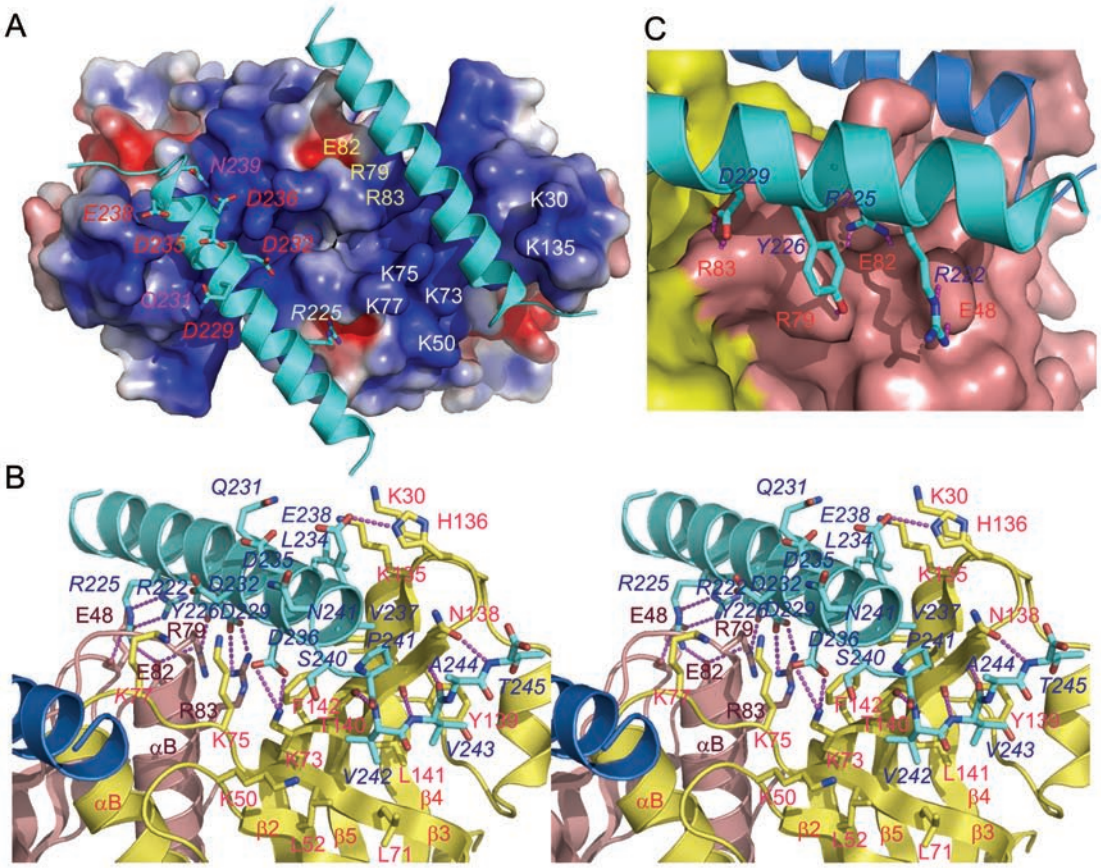

D

$Cdc13_{OB1}$	$Pol1_{CBM}$	K_d (μM)
WT	WT	3.8 ± 0.5
WT	D229R	nd
WT	L233R	nd
WT	D236R	nd
WT	V237A	nd
WT	P241A	nd
WT	V242R	nd
R79E	WT	nd
R83E	WT	nd
3K-3E (K73E/K75E/K77E)	WT	nd
I32E	WT	nd
V133E	WT	nd
T140E	WT	nd
F142A	WT	nd

E

$Cdc13_{OB1}$	$Pol1_{CBM}$	K_d (μM)
WT	WT	3.8 ± 0.5
L84R	WT	12.0 ± 3.5
I87R	WT	nd
L91R	WT	nd
Y95R	WT	nd

F

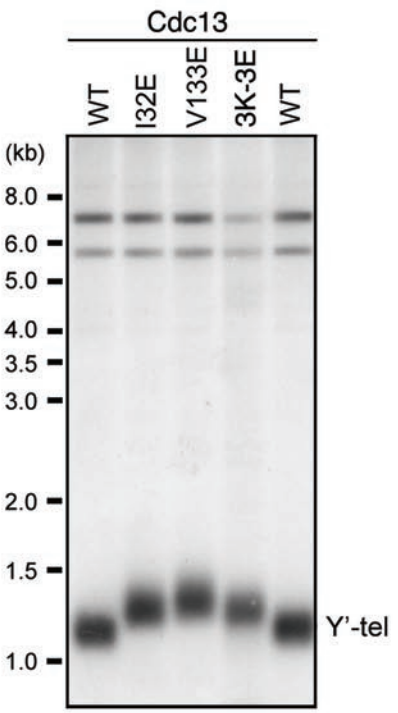

using ITC. In support of the crystal structure, $Cdc13_{OB1}$ mutations of either the hydrophobic residues (Ile32, Val133, Thr140, or Phe142) at the bottom of the groove or the basic residues (K73E/K75E/K77E, R79E, and R83E) at the periphery were sufficient to eliminate the interaction (Figure 6D). Similarly, mutations of the hydrophobic or acidic residues of $Pol1_{CBM}$ on the other side of the interface also completely abolished the interaction (Figure 6D). Taken together, we conclude that both the electrostatic and hydrophobic interactions observed in the crystal structure are important for the interaction between $Cdc13_{OB1}$ and $Pol1_{CBM}$.

Notably, mutations of residues in both Cdc13 and Pol1 ($Pol1_{CBM}$ D229R, and $Cdc13_{OB1}$ R79E and R83E) at the interface between $Pol1_{CBM}$ and the second $Cdc13_{OB1}$ molecule in the dimer were also able to completely disrupt the $Cdc13_{OB1}$-$Pol1_{CBM}$ interaction (Figure 6D). This observation promoted us to examine the role of Cdc13 dimerization in Pol1 binding in solution. As shown in Figure 6E, all four monomeric mutants of $Cdc13_{OB1}$ exhibited complete or partial loss of Pol1 association in a manner that is entirely consistent with the severity of the dimerization defects (Figure 2D, 2E and 2F). In particular, the L84R mutant, which retained partial function in dimerization, also exhibited the mildest Pol1 association defect (Figure 6E). Therefore, we conclude that Cdc13 dimerization is a prerequisite for the stable association between Cdc13 and Pol1.

Loss of the Cdc13-Pol1 interaction, but not Cdc13 dimerization, results in telomere lengthening

Previous investigations demonstrated that loss of the Cdc13-Pol1 interaction by substitution of wild-type Pol1 with Cdc13-binding-deficient mutants was often correlated with telomere lengthening [10, 11]. The telomere shortening phenotype of the dimerization-deficient *CDC13* mutants was thus somewhat surprising, given the mutant's lack of Pol1 binding (Figure 4B). One explanation for this apparent discrepancy is that the dimerization of Cdc13 not only disrupts the Cdc13-Pol1 interaction but may also affect the binding of Cdc13 to other partners such as Imp4 and Sir4. We predicted that Cdc13 mutations that only disrupt the Cdc13-Pol1 interface but not the dimerization of Cdc13 would cause telomere lengthening, similar to the phenotype caused by the Pol1 mutants [10, 11]. To test this idea, we introduced several mutations in Cdc13 to reduce Pol1 binding (I32E, V133E, and K73E/K75E/K77E (3K-3E)) and analyzed the telomere length phenotypes of the resulting mutants. Strains carrying these *CDC13* mutants grew as well as wild-type cells at 25 °C, 30 °C, and 37 °C (Supplementary information, Figure S5A). Thus, none of the mutant alleles eliminated an essential function of Cdc13. Notably, as we predicted, all three mutants yielded longer telomeres, similar to those caused by the Cdc13-binding-deficient mutants of Pol1 (Figure 6F) [10, 11]. The differences in telomere lengths are unlikely to be caused by differences in the abundance of Cdc13 in cells, as western analysis showed that each of the mutant alleles produced nearly wild-type levels of Cdc13 (Supplementary information, Figure S5B). Clearly, disruption of Cdc13 dimerization caused defects that are distinct from the disruption of Cdc13-Pol1 interface. We therefore suggest that dimerization is likely to affect at least one other function or interaction mediated by Cdc13. Indeed, many other interaction partners for Cdc13 have been identified, and knowing the effect of dimerization on each interaction will be necessary to fully understand the role of dimerization on Cdc13 function.

Dimerization is a conserved feature of Cdc13 proteins

Multiple sequence alignment revealed a high degree

Figure 6 The $Cdc13_{OB1}$-$Pol1_{CBM}$ interface. **(A)** Electrostatic interaction at the $Cdc13_{OB1}$-$Pol1_{CBM}$ interface. The interaction surfaces are complementary in charge distribution and in their van der Waals contours. The $Cdc13_{OB1}$ dimer is in surface representation and colored according to its electrostatic potential. The two $Pol1_{CBM}$ peptides are in ribbon representation and colored in cyan. Acidic (in red) and polar (in pink) residues are shown as stick models in one $Pol1_{CBM}$ peptide at left in the complex. The basic residues of $Cdc13_{OB1}$ at the interface are labeled in white (residues of $Cdc13_{OB1}$ at right in the complex) and in yellow (residues of $Cdc13_{OB1}$ at left in the complex). **(B)** Stereo view of the $Cdc13_{OB1}$-$Pol1_{CBM}$ interface. $Cdc13_{OB1}$- and $Pol1_{CBM}$-interacting residues are presented as stick models. The $Cdc13_{OB1}$-$Pol1_{CBM}$ intermolecular hydrogen bonds are shown as dashed magenta lines. **(C)** $Pol1_{CBM}$ interacts with both $Cdc13_{OB1}$ subunits in the dimer. The C-terminal half of the $Pol1_{CBM}$ helix (residues 216-229) binds into a depression from the opposing $Cdc13_{OB1}$ molecule in the dimer. $Pol1_{CBM}$ is colored in cyan and residues 216-229 are shown as stick models. The two $Cdc13_{OB1}$ subunits are in surface representation and colored in yellow and salmon, respectively. **(D)** *In vitro* ITC binding of seven $Cdc13_{OB1}$ mutants and six $Pol1_{CBM}$ mutants with wild-type $Pol1_{CBM}$ and $Cdc13_{OB1}$, respectively. **(E)** *In vitro* ITC binding of four $Cdc13_{OB1}$ mutants that have defects in $Cdc13_{OB1}$ homodimerization with wild-type $Pol1_{CBM}$. **(F)** Chromosomal DNAs were prepared from strains bearing wild-type or CDC13 mutants that are deficient in Pol1 interaction, digested with *Xho*I, and subjected to Southern blot analysis using a labeled fragment from the subtelomeric Y' element as the probe. The differences in the telomere patterns of these assays and those shown in Figure 4B are due to differences in the restriction enzymes and probes used.

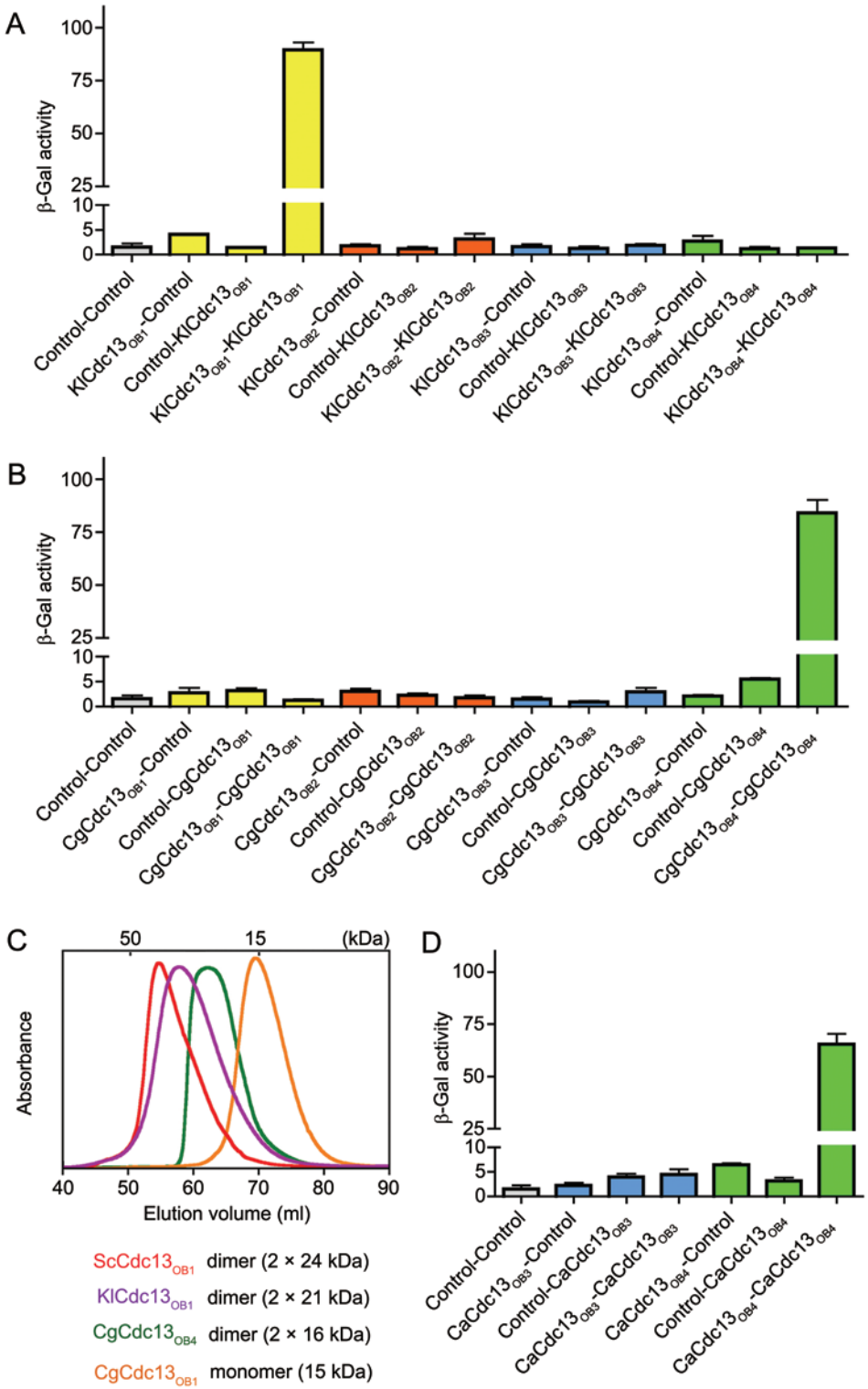

Figure 7 Cdc13 proteins employ either the N-terminal OB1 or the C-terminal OB4 domain for dimerization. **(A**, **B**, **D)** Self-association of each OB fold of *Kl*Cdc13 **(A)**, *Cg*Cdc13 **(B)**, and *Ca*Cdc13 **(D)** was examined in yeast two-hybrid assays. The color scheme of the OB folds is the same as in Figure 1. Self-association was reflected by the level of β-galactosidase activity produced by the reporter gene. Data are averages of three independent β-galactosidase measurements normalized to the dimeric interaction of the OB1 domain of *Sc*Cdc13 shown in Supplementary information, Figure S2C, arbitrarily set to 100. **(C)** Superposed gel-filtration profiles of *Sc*Cdc13$_{OB1}$, *Kl*Cdc13$_{OB1}$, *Cg*Cdc13$_{OB4}$, and *Cg*Cdc13$_{OB1}$.

of conservation in most of the residues important for homodimerization of *Sc*Cdc13$_{OB1}$, suggesting that dimerization through the first OB fold is probably conserved for *Saccharomyces* and *Kluyveromyces* Cdc13 proteins (Supplementary information, Figure S1). To test this idea, we examined the oligomeric state of different OB fold domains of *Kluyveromyces lactis* Cdc13 (*Kl*Cdc13). Even though the putative dimerization interface of *Kl*Cdc13 only shares modest sequence similarity with *Sc*Cdc13, yeast two-hybrid experiments clearly revealed self-interaction by the N-terminal OB1 domain of *Kl*Cdc13 (Figure 7A), strongly supporting the notion that dimerization is a conserved feature of *Saccharomyces* and *Kluyveromyces* Cdc13 proteins.

A notable standout in our sequence alignment was *Candida glabrata* Cdc13 (*Cg*Cdc13), whose OB1 domain has a shorter αB helix and does not contain the conserved residues for dimerization (Supplementary information, Figure S1). (It should be noted that *Candida glabrata*, despite its name, is evolutionarily closer to *Saccharomyces* and *Kluyveromyces* than other *Candida* spp.) In keeping with the alignment, *Cg*Cdc13$_{OB1}$ failed to self-associate in the yeast two-hybrid assay (Figure 7B). Strikingly, the predicted C-terminal OB fold of *Cg*Cdc13, *Cg*Cdc13$_{OB4}$, exhibited a strong self-association activity (Figure 7B). By contrast, both *Sc*Cdc13$_{OB4}$ and *Kl*Cdc13$_{OB4}$ behaved as monomers in yeast cells (Supplementary information, Figure S2E and Figure 7A). To further assess the dimerization of the OB folds in different Cdc13 proteins *in vitro*, recombinant *Kl*Cdc13$_{OB1}$, *Cg*Cdc13$_{OB1}$, and *Cg*Cdc1$_{OB4}$ proteins were purified and individually subjected to gel-filtration chromatography. As shown in Figure 7C, the apparent molecular weights of these domains, based on the gel-filtration profiles, are entirely consistent with the yeast two-hybrid results.

Our previous studies showed that Cdc13 homologs in many *Candida* spp. are considerably smaller and lack the N-terminal half of their *S. cerevisiae* counterpart [23]. These *Candida* spp. cluster evolutionarily and form a well-defined clade (Supplementary information, Figure S6). Sequence alignments suggest that these Cdc13 homologs only contain two OB folds, which correspond to OB3 and OB4 in *Saccharomyces* spp. Cdc13 proteins [23, 40]. Therefore, in keeping with the nomenclature of Cdc13, we refer to the two OB folds of *Candida* Cdc13 proteins as OB3 and OB4, respectively. Given that these smaller Cdc13 proteins lack OB1, we hypothesized that like *Cg*Cdc13, they might form dimeric structures through their OB4 domains. Hence, we examined the oligomeric states of the two OB folds of *Candida albicans* Cdc13 (*Ca*Cdc13). As predicted, *Ca*Cdc13$_{OB4}$, but not the putative DNA-binding domain *Ca*Cdc13$_{OB3}$, associated with itself (Figure 7D). Taken together, we propose that homodimerization is likely to be a conserved feature of Cdc13 proteins in all yeast species in the Saccharomycotina linage; except for *Cg*Cdc13, *Saccharomyces*-like large Cdc13 proteins form dimers through their N-terminal OB1 domains, whereas *Candida*-like small Cdc13 proteins and *Cg*Cdc13 form dimers through their C-terminal OB4 domains.

Discussion

It has been proposed that CST is a telomere-specific RPA-like complex [12]. Recent structural studies by us and other groups demonstrated a close structural resemblance between Stn1-Ten1 and RPA32-RPA14 [22, 23]. Although the solution structure of the DNA-binding OB fold of Cdc13 is available, the relationship between Cdc13 and RPA70 remains unclear due to the lack of structural information on other regions of Cdc13 and the lack of sequence similarity between Cdc13 and RPA. In this work, our bioinformatic and structural analyses provide the first direct evidence for the existence of multiple OB folds in Cdc13, which is characteristic of RPA70. The similarity between the Cdc13$_{OB1}$-Pol1$_{CBM}$ and the RPA70N-p53 complexes further extends the parallel between Cdc13 and RPA70 (Figure 4C and 4D). However, despite these similarities, there are substantial differences between Cdc13 and RPA70. First, unlike Stn1-Ten1, none of the two structurally defined OB folds of Cdc13 show similarity to their counterparts in RPA70 outside the central β-barrel cores (Figure 2B) [25, 26]. Second, the two central OB folds of RPA70 are required for efficient DNA binding, whereas Cdc13 uses just its OB3 for binding [41]. These marked differences suggest that the resemblance between Cdc13 and RPA70 may be the result of convergent evolution. In other words, Cdc13 may not have evolved from the ancestral RPA70, but were instead recruited by the Stn1-Ten1 complex to provide single-stranded DNA-binding activity. In keeping with this idea, we found that *Candida* spp. Cdc13 proteins contain only two OB folds that correspond to the C-terminal half of *Saccharomyces* spp. proteins. In addition, the recently identified CTC1 proteins, the largest components in the human and plant CST complexes, are much larger proteins and show no sequence similarity to either Cdc13 or RPA70, supporting the disparate origins of these proteins [17, 18]. While we cannot rule out the possibility that a common origin for these proteins is obscured by extremely rapid evolutionary divergence, it seems clear that the structural and functional relationships between Cdc13/CTC1 and Stn1-Ten1 are quite distinct from those between RPA70 and RPA32-14.

One striking result of this study is that homodimerization appears to be a conserved feature of Cdc13. Except for *Cg*Cdc13, most *Saccharomyces* and *Kluyveromyces* Cdc13 proteins form dimers through their N-terminal OB1 domains. In contrast, homodimerization of *Candida* Cdc13 proteins and *Cg*Cdc13 is mediated by the C-terminal OB fold. The use of OB4 for dimerization by *Cg*Cdc13 is somewhat surprising, given the closer kinship of this yeast to *Saccharomyces* than to *Candida* spp. Perhaps this represents another case of convergent evolution. For example, an accidental loss of OB1 dimerization by *Cg*Cdc13 may have provided the selection pressure for the evolution of other dimerization mechanisms, resulting eventually in the utilization of OB4. The prevalence of Cdc13 dimerization suggests that this property may facilitate interaction of Cdc13 with multiple targets. For example, one established function of OB1 dimerization is to facilitate the interaction with Pol1; our mutagenesis data clearly showed that dimerization of *Sc*Cdc13 OB1 domain is required for Pol1 binding. The significance of OB4 dimerization is less clear. A possible function for the dimerization of this domain is suggested by the homodimerization of many telomere-binding proteins such as fission yeast Taz1 and human TRF1 and TRF2 [42-46]. Because of the low intrinsic affinity of individual DNA-binding domains, these proteins require dimerization for stable telomere DNA interaction [42, 44, 46]. Thus, even though the *S. cerevisiae* Cdc13 can clearly bind DNA as a monomer, it is possible that dimerization of the smaller Cdc13 proteins in *Candida* spp. may enhance their DNA-binding activity. Indeed, we found recently that the OB_{DBD} of *Ct*Cdc13 interacts weakly with the cognate telomere repeat and requires the OB4 domain for high-affinity DNA binding (EYY and NL, manuscript in preparation). Yet another potential function for Cdc13 dimerization is suggested by the reported multimerization of the telomerase complex. Although the data are somewhat inconclusive, both yeast and human telomerase have been proposed to function as dimmers [47, 48]. Because Cdc13 is known to interact with the Est1 component of yeast telomerase, dimerization of Cdc13 could help bring two telomerase complexes into close vicinity for proper function. Further studies are needed to test these possibilities and reveal the full functional significance of Cdc13 dimerization in regulating and maintaining budding yeast telomeres.

Materials and Methods

Protein expression and purification

S. cerevisiae $Cdc13_{OB1}$ (residues 12-243) and $Pol1_{CBM}$ (residues 215-250) were cloned into a modified pET28b vector with a Sumo protein fused at the N-terminus after the His_6 tag [49]. They were expressed in *E. coli* BL21 (DE3). After induction for 16 h with 0.1 mM IPTG at 20 °C, the cells were harvested by centrifugation and the pellets were resuspended in lysis buffer (50 mM Tris-HCl (pH 8.0), 50 mM NaH_2PO_4, 400 mM NaCl, 3 mM imidazole, 10% glycerol, 1 mM PMSF, 0.1 mg/ml lysozyme, 2 mM 2-mercaptoethanol, and homemade protease inhibitor cocktail). The cells were then lysed by sonication and the cell debris was removed by ultracentrifugation. The supernatant was mixed with Ni-NTA agarose beads (Qiagen) and rocked for 2 h at 4 °C before elution with 250 mM imidazole. Then, Ulp1 protease was added to remove the His_6-Sumo tag for 12 h at 4 °C. $Cdc13_{OB1}$ was then further purified by passage through Mono-Q ion exchange column and by gel-filtration chromatography on a Hiload Superdex75 (GE Healthcare) equilibrated with 25 mM Tris-HCl (pH 8.0), 150 mM NaCl, and 5 mM dithiothreitol (DTT). $Pol1_{CBM}$ was further purified by gel-filtration chromatography on Hiload Superdex75 column equilibrated with 100 mM ammonium bicarbonate. The purified $Cdc13_{OB1}$ was concentrated to 20 mg/ml and stored at −80 °C. The purified $Pol1_{CBM}$ peptide was concentrated by SpeedVac and then lyophilized. The lyophilization products were then resuspended in water at a concentration of 50 mg/ml and stored at −80 °C.

Crystallization, data collection, and structure determination

***S. cerevisiae* $Cdc13_{OB1}$** Crystals were grown at 4 °C by the sitting drop vapor diffusion method. The precipitant/well solution contained 21% PEG3350, 0.2 M NaCl, 0.1 M HEPES (pH 7.0), and 10 mM DTT. Heavy-atom derivatives were obtained by soaking crystals in a solution containing 30% PEG3350, 0.2 M NaCl, 0.1 M HEPES (pH 7.0) and 0.1 mM MeHgAc for 3 h and back-soaking for 2 h in 30% PEG3350, 0.2 M NaCl, and 0.1 M HEPES (pH 7.0). Both native and heavy-atom-derivative crystals were gradually transferred into a harvesting solution (30% PEG3350, 0.2 M NaCl, 0.1 M HEPES (pH 7.00), and 20% glycerol) before being flash frozen in liquid nitrogen for storage and data collection under cryogenic conditions (100 K). Native and Hg-SAD (at Hg peak wavelength) data sets were collected at APS beamline 21ID-D and processed using HKL2000 [50]. Crystals belong to space group $P2_12_12$ and contain one $Cdc13_{OB1}$ molecule per asymmetric unit. Native crystals diffracted to 2.5 Å resolution with cell parameter a = 62.515 Å, b = 68.641 Å and c = 52.815 Å. Three mercury sites were located and refined, and the SAD phases calculated using SHARP [51]. The initial SAD map was significantly improved by solvent flattening. A model was automatically built into the modified experimental electron density using ARP/WARP [52]. The model was then transferred into the native unit cell by rigid-body refinement and further refined using simulated annealing and positional refinement in CNS [53], with manual rebuilding using program O [54].

***S. cerevisiae* $Cdc13_{OB1}$-$Pol1_{CBM}$** $Cdc13_{OB1}$ (20 mg/ml) and $Pol1_{CBM}$ (50 mg/ml) were mixed together in a molecular ratio of 1:1. Crystals were grown at 4 °C by sitting drop vapor diffusion method. The precipitant/well solution contained 23% PEG3350 and 0.2 M magnesium formate, 0.1 M Tris-HCl (pH 8.0), and 5 mM DTT. Crystals were gradually transferred into a harvesting solution (25% PEG3350, 0.2 M magnesium formate, 0.1 M Tris-HCl (pH 8.0), 5 mM DTT, and 25% glycerol) before being flash frozen in liquid nitrogen for storage and data collection under cryogenic conditions. Native data set with a resolution of 2.4 Å was collected at APS beamline 21ID-D and processed using HKL2000 [50]. The

crystal belongs to space group $P2_12_12_1$, with unit cell parameters a = 60.393 Å, b = 85.090 Å, and c = 60.376 Å. The structure was determined with the molecular replacement method using Phaser program [55]. Two Pol1 peptides could be identified and modeled unambiguously in the complex. Model building and refinement were carried out following the same procedure as those for Cdc13$_{OB1}$, as described for Cdc13$_{OB1}$.

Cross-linking assay

Chemical cross-linking experiment was performed with purified Cdc13$_{OB1}$ and full-length Cdc13 in PBS buffer. Cross-linking reagent stock solution was prepared by dissolving 35 mg EDC (3-dimethylaminopropyl carbodiimide hydrochloride, Thermo Scientific) into 532 µl distilled water. Serial two-fold dilutions were made by mixing EDC stock solution with distilled water. A measure of 3 µg of Cdc13$_{OB1}$ or full-length Cdc13 was mixed with 1 µl EDC solution and incubated at room temperature for 30 min. The reaction was quenched by adding 1 M Tris-HCl (pH 8.0) to a final concentration of 50 mM and incubated at room temperature for 15 min. The reaction mixture was then subjected to SDS-PAGE analysis.

Yeast two-hybrid assay

The yeast two-hybrid assays were performed using L40 strain harboring pBTM116 and PACT2 (Clontech) fusion plasmids. Colonies containing both plasmids were selected on –Leu –Trp plates. β-Galactosidase activities were measured by a liquid assay [56].

Sucrose gradient sedimentation

Sucrose gradient ultracentrifugation of Cdc13 was performed with a 10%-35% (v/v) discontinuous sucrose density gradient. Cdc13 was loaded onto the gradient and then centrifuged at 182 000 × *g* for 16 h at 4 °C in a SW 41Ti swinging bucket rotor and Optima XL-90 ultracentrifuge (Beckman Instruments). In all, 300 µl each of the fractions were collected from the top. Calibration was done with aldolase, catalase, and ferritin (Amersham).

Co-immunoprecipitation

Yeast cells harboring both HA-tagged and LexA$_{BD}$-tagged Cdc13 proteins were used to analyze the homodimerization of Cdc13. Anti-HA antibody was added to the total yeast extract (~500 µg) in buffer A (50 mM Tris-HCl (pH 7.5), 1 mM EDTA, 50 mM NaOAc, 1 mM DTT, 1× protease inhibitor cocktail (Calbiochem), 0.1% Tween 20, and 20% glycerol) and mixed at 4 °C for 1 h. A 50 µl aliquot of protein A-Sepharose 4B beads was added to the mixture, followed by continued incubation for another 1 h. The beads were then washed three times with buffer A. The immunoprecipitates were eluted with 0.1 M citric acid (pH 3.0) and then subjected to SDS-PAGE analysis. Anti-LexA antibody was used in western blotting analysis to detect the presence of LexA$_{BD}$-Cdc13 in the IP samples.

Complementation of cdc13Δ by CDC13 OB1 mutants

Plasmid loss experiments were carried out to test whether *CDC13* OB1 mutants are sufficient to complement the essential functions of a *cdc13*Δ mutation. Briefly, the mutations were introduced into the pTHA-NLS-CDC13 plasmid using a QuikChange protocol. The plasmids bearing either the wild-type or mutant *CDC13* genes were transformed into the YJL501 (cdc13Δ::HIS3/YEP24-CDC13) strain, which contains a plasmid carrying CDC13 (YEP24-CDC13) for viability. The resulting transformants were spotted on plates containing 0.5 mg/ml 5-fluoroorotic acid and incubated at different temperatures until colonies formed (~48 h).

Telomere length determination

To determine telomere length, yeast DNA was prepared, digested with either *Pst*I or *Xho*I, and separated on 1% agarose gels. The DNA fragments were transferred to a Hybond N+ filter (Amersham) for hybridization using either a fragment from the Y' element or poly(dG-dT) • poly(dC-dA) as the probe.

Acknowledgments

We thank Y Chen and W Deng (University of Michigan, USA) for help at various stages of the project. This work was supported by NIH grants (GM 083015-01 to ML, and GM062631 to NL), an American Cancer Society Research Scholar grant (to ML), NSC 97-2311-B-010-005 from Taiwan National Science Council and NHRI-EX98-9625SI from Taiwan National Health Research Institute (to JL), and Public Service Grant DK074270 (to BCF). ML is a Howard Hughes Medical Institute Early Career Scientist. Use of Life Sciences Collaborative Access Team Sector 21 was supported by the Michigan Economic Development Corporation and the Michigan Technology Tri-Corridor (Grant 085P1000817). Use of the Advanced Photon Source was supported by the US Department of Energy, Office of Science, Office of Basic Energy Sciences, under contract no. DE-AC02-06CH11357.

References

1 Bertuch AA, Lundblad V. The maintenance and masking of chromosome termini. *Curr Opin Cell Biol* 2006; **18**:247-253.
2 de Lange T. How telomeres solve the end-protection problem. *Science* 2009; **326**:948-952.
3 Autexier C, Lue NF. The structure and function of telomerase reverse transcriptase. *Annu Rev Biochem* 2006; **75**:493-517.
4 Collins K. The biogenesis and regulation of telomerase holoenzymes. *Nat Rev Mol Cell Biol* 2006; **7**:484-494.
5 Osterhage JL, Friedman KL. Chromosome end maintenance by telomerase. *J Biol Chem* 2009; **284**:16061-16065.
6 Lundblad V. Telomeres in the '80s: a few recollections. *Nat Struct Mol Biol* 2006; **13**:1036-1038.
7 Eldridge AM, Wuttke DS. Probing the mechanism of recognition of ssDNA by the Cdc13-DBD. *Nucleic Acids Res* 2008; **36**:1624-1633.
8 Hughes TR, Weilbaecher RG, Walterscheid M, Lundblad V. Identification of the single-strand telomeric DNA binding domain of the *Saccharomyces cerevisiae* Cdc13 protein. *Proc Natl Acad Sci USA* 2000; **97**:6457-6462.
9 Pennock E, Buckley K, Lundblad V. Cdc13 delivers separate complexes to the telomere for end protection and replication. *Cell* 2001; **104**:387-396.
10 Qi H, Zakian VA. The *Saccharomyces* telomere-binding protein Cdc13p interacts with both the catalytic subunit of DNA polymerase alpha and the telomerase-associated est1 protein. *Genes Dev* 2000; **14**:1777-1788.
11 Hsu CL, Chen YS, Tsai SY, Tu PJ, Wang MJ, Lin JJ . Interac-

tion of *Saccharomyces* Cdc13p with Pol1p, Imp4p, Sir4p and Zds2p is involved in telomere replication, telomere maintenance and cell growth control. *Nucleic Acids Res* 2004; **32**:511-521.
12 Gao H, Cervantes RB, Mandell EK, Otero JH, Lundblad V. RPA-like proteins mediate yeast telomere function. *Nat Struct Mol Biol* 2007; **14**:208-214.
13 Grossi S, Puglisi A, Dmitriev PV, Lopes M, Shore D. Pol12, the B subunit of DNA polymerase alpha, functions in both telomere capping and length regulation. *Genes Dev* 2004; **18**:992-1006.
14 Petreaca RC, Chiu HC, Eckelhoefer HA, Chuang C, Xu L, Nugent CI. Chromosome end protection plasticity revealed by Stn1p and Ten1p bypass of Cdc13p. *Nat Cell Biol* 2006; **8**:748-755.
15 Puglisi A, Bianchi A, Lemmens L, Damay P, Shore D. Distinct roles for yeast Stn1 in telomere capping and telomerase inhibition. *EMBO J* 2008; **27**:2328-2339.
16 Martin V, Du LL, Rozenzhak S, Russell P. Protection of telomeres by a conserved Stn1-Ten1 complex. *Proc Natl Acad Sci USA* 2007; **104**:14038-14043.
17 Miyake Y, Nakamura M, Nabetani A, *et al*. RPA-like mammalian Ctc1-Stn1-Ten1 complex binds to single-stranded DNA and protects telomeres independently of the Pot1 pathway. *Mol Cell* 2009; **36**:193-206.
18 Surovtseva YV, Churikov D, Boltz KA, *et al*. Conserved telomere maintenance component 1 interacts with STN1 and maintains chromosome ends in higher eukaryotes. *Mol Cell* 2009; **36**:207-218.
19 Wan M, Qin J, Songyang Z, Liu D. OB fold-containing protein 1 (OBFC1), a human homolog of yeast Stn1, associates with TPP1 and is implicated in telomere length regulation. *J Biol Chem* 2009; **284**:26725-26731.
20 Wold MS. Replication protein A: a heterotrimeric, single-stranded DNA-binding protein required for eukaryotic DNA metabolism. *Annu Rev Biochem* 1997; **66**:61-92.
21 Bochkarev A, Bochkareva E. From RPA to BRCA2: lessons from single-stranded DNA binding by the OB-fold. *Curr Opin Struct Biol* 2004; **14**:36-42.
22 Gelinas AD, Paschini M, Reyes FE, *et al*. Telomere capping proteins are structurally related to RPA with an additional telomere-specific domain. *Proc Natl Acad Sci USA* 2009; **106**:19298-19303.
23 Sun J, Yu EY, Yang Y, *et al*. Stn1-Ten1 is an Rpa2-Rpa3-like complex at telomeres. *Genes Dev* 2009; **23:**2900-2914.
24 Theobald DL, Wuttke DS. Prediction of multiple tandem OB-fold domains in telomere end-binding proteins Pot1 and Cdc13. *Structure* 2004; **12**:1877-1879.
25 Bochkarev A, Pfuetzner RA, Edwards AM, Frappier L. Structure of the single-stranded-DNA-binding domain of replication protein A bound to DNA. *Nature* 1997; **385**:176-181.
26 Mitton-Fry RM, Anderson EM, Hughes TR, Lundblad V, Wuttke DS. Conserved structure for single-stranded telomeric DNA recognition. *Science* 2002; **296**:145-147.
27 Rost B, Yachdav G, Liu J. The PredictProtein server. *Nucleic Acids Res* 2004; **32**:W321-W326.
28 Bochkareva E, Kaustov L, Ayed A, *et al*. Single-stranded DNA mimicry in the p53 transactivation domain interaction with replication protein A. *Proc Natl Acad Sci USA* 2005; **102**:15412-15417.
29 Bochkareva E, Korolev S, Lees-Miller SP, Bochkarev A. Structure of the RPA trimerization core and its role in the multistep DNA-binding mechanism of RPA. *EMBO J* 2002; **21**:1855-1863.
30 Fanning E, Klimovich V, Nager AR. A dynamic model for replication protein A (RPA) function in DNA processing pathways. *Nucleic Acids Res* 2006; **34**:4126-4137.
31 Arcus V. OB-fold domains: a snapshot of the evolution of sequence, structure and function. *Curr Opin Struct Biol* 2002; **12**:794-801.
32 Theobald DL, Mitton-Fry RM, Wuttke DS. Nucleic acid recognition by OB-fold proteins. *Annu Rev Biophys Biomol Struct* 2003; **32**:115-133.
33 Theobald DL, Wuttke DS. Divergent evolution within protein superfolds inferred from profile-based phylogenetics. *J Mol Biol* 2005; **354:**722-737.
34 Jacobs DM, Lipton AS, Isern NG, *et al*. Human replication protein A: global fold of the N-terminal RPA-70 domain reveals a basic cleft and flexible C-terminal linker. *J Biomol NMR* 1999; **14**:321-331.
35 Holm L, Sander C. Database algorithm for generating protein backbone and side-chain co-ordinates from a C alpha trace application to model building and detection of co-ordinate errors. *J Mol Biol* 1991; **218**:183-194.
36 Mitton-Fry RM, Anderson EM, Theobald DL, Glustrom LW, Wuttke DS. Structural basis for telomeric single-stranded DNA recognition by yeast Cdc13. *J Mol Biol* 2004; **338**:241-255.
37 Horvath MP, Schweiker VL, Bevilacqua JM, Ruggles JA, Schultz SC. Crystal structure of the Oxytricha nova telomere end binding protein complexed with single strand DNA. *Cell* 1998; **95**:963-974.
38 Lei M, Podell ER, Baumann P, Cech TR. DNA self-recognition in the structure of Pot1 bound to telomeric single-stranded DNA. *Nature* 2003; **426**:198-203.
39 Lei M, Podell ER, Cech TR. Structure of human POT1 bound to telomeric single-stranded DNA provides a model for chromosome end-protection. *Nat Struct Mol Biol* 2004; **11**:1223-1229.
40 Lue NF. Plasticity of telomere maintenance mechanisms in yeast. *Trends Biochem Sci* 2010; **35**:8-17.
41 Anderson EM, Halsey WA, Wuttke DS. Delineation of the high-affinity single-stranded telomeric DNA-binding domain of Saccharomyces cerevisiae Cdc13. *Nucleic Acids Res* 2002; **30**:4305-4313.
42 Bianchi A, Smith S, Chong L, Elias P, de Lange T. TRF1 is a dimer and bends telomeric DNA. *EMBO J* 1997; **16**:1785-1794.
43 Broccoli D, Smogorzewska A, Chong L, de Lange T. Human telomeres contain two distinct Myb-related proteins, TRF1 and TRF2. *Nat Genet* 1997; **17**:231-235.
44 Konishi A, de Lange T. Cell cycle control of telomere protection and NHEJ revealed by a ts mutation in the DNA-binding domain of TRF2. *Genes Dev* 2008; **22**:1221-1230.
45 Fairall L, Chapman L, Moss H, de Lange T, Rhodes D. Structure of the TRFH dimerization domain of the human telomeric proteins TRF1 and TRF2. *Mol Cell* 2001; **8**:351-361.
46 Spink KG, Evans RJ, Chambers A. Sequence-specific binding

of Taz1p dimers to fission yeast telomeric DNA. *Nucleic Acids Res* 2000; **28**:527-533.
47 Prescott J, Blackburn EH. Functionally interacting telomerase RNAs in the yeast telomerase complex. *Genes Dev* 1997; **11**:2790-2800.
48 Wenz C, Enenkel B, Amacker M, Kelleher C, Damm K, Lingner J. Human telomerase contains two cooperating telomerase RNA molecules. *EMBO J* 2001; **20**:3526-3534.
49 Wang F, Podell ER, Zaug AJ, *et al*. The POT1-TPP1 telomere complex is a telomerase processivity factor. *Nature* 2007; **445**:506-510.
50 Otwinowski Z, Minor W. Processing of X-ray diffraction data collected in oscillation mode. In: *Methods in Enzymology*, vol. 276. Academic Press, 1997:307-326.
51 La Fortelle ED, Bricogne G. Maximum-likelihood heavy-atom parameter refinement for multiple isomorphous replacement and multiwavelength anomalous diffraction methods. In: *Methods in Enzymology*, vol. 276. Academic Press, 1997:472-494.
52 Lamzin VS, Perrakis A, Wilson KS. The ARP/WARP suite for automated construction and refinement of protein models. In: Rossmann MG, Arnold E, eds. International Tables for Crystallography. Volume F: Crystallography of Biological Macromolecules. Dordrecht, The Netherlands: Kluwer Academic Publishers, 2001:720-722.
53 Brunger AT, Adams PD, Clore GM, *et al*. Crystallography & NMR system: a new software suite for macromolecular structure determination. *Acta Crystallogr D Biol Crystallogr* 1998; **54**:905-921.
54 Jones TA, Zou JY, Cowan SW, Kjeldgaaed M. Improved methods for building protein models in electron density maps and the location of errors in these methods. *Acta Crystallogr A* 1991; **47**:110-119.
55 McCoy AJ, Grosse-Kunstleve RW, Adams PD, Winn MD, Storoni LC, Read RJ, *et al*. Phaser crystallographic software. *J Appl Crystallogr* 2007; **40**:658-674.
56 Moretti P, Freeman K, Coodly L, Shore D. Evidence that a complex of SIR proteins interacts with the silencer and telomere-binding protein RAP1. *Genes Dev* 1994; **8**:2257-2269.

(**Supplementary information** is linked to the online version of the paper on the *Cell Research* website.)